Strain field in (Ga,Mn)As/GaAs periodic wires revealed by coherent X-ray diffraction

2011 EPL 94 66001

(http://iopscience.iop.org/0295-5075/94/6/66001)

A Letters Journal Exploring the Frontiers of Physics

June 2011

EPL, **94** (2011) 66001
doi: 10.1209/0295-5075/94/66001

www.epljournal.org

Strain field in (Ga,Mn)As/GaAs periodic wires revealed by coherent X-ray diffraction

A. A. Minkevich[1(a)], E. Fohtung[1], T. Slobodskyy[1], M. Riotte[1], D. Grigoriev[1], T. Metzger[2], A. C. Irvine[3], V. Novák[4], V. Holý[5] and T. Baumbach[1]

[1] *ANKA-Institute for Synchrotron radiation, Karlsruhe Institute of Technology - 76344 Eggenstein-Leopoldshafen, Germany, EU*
[2] *Max Planck Institute of colloids and interfaces, Department of Biomaterials - 14424 Potsdam-Golm, Germany, EU*
[3] *Microelectronics Research Centre, Cavendish Laboratory, University of Cambridge - Cambridge CB3 0HE, UK, EU*
[4] *Institute of Physics of the ASCR - Cukrovarnicka 10, 162 00 Praha, Czech Republic, EU*
[5] *Department of Condensed Matter Physics, Faculty of Mathematics and Physics, Charles University Ke Karlovu 5, 121 16 Praha, Czech Republic, EU*

received 14 April 2011; accepted in final form 6 May 2011
published online 26 May 2011

PACS 61.05.cp – X-ray diffraction
PACS 62.20.-x – Mechanical properties of solids
PACS 42.30.-d – Imaging and optical processing

Abstract – An experimental and simulation study of the full strain tensor and of strain-induced magnetocrystalline anisotropies in arrays of lithographically patterned (Ga,Mn)As on GaAs(001) is performed using a coherent diffraction lensless microscopy technique. We demonstrate the ability of our technique to get an insight into the strain field propagating in the crystal part belonging to the substrate. The experimentally reconstructed strain fields are in good agreement with those obtained from simulations based on elasticity theory.

Introduction. – The necessity to understand the distribution of elastic strain in crystalline nano- and micro-systems has been fueled by the recent discovery of the role played by strain in the functionality of semiconductor devices [1–4]. Relatively large dielectric polarization effects can be detected in the presence of the strain gradients in crystals [5,6]. In systems consisting of magnetic crystals the strain distribution, if spatially tuned, can be used to control the resultant magnetic anisotropy [7]. In spintronic device materials, the interplay between anisotropies of magnetic and transport properties combined with the intrinsic elastic strain in the epitaxial layers give rise to multiple device relevant effects such as strong anisotropic magnetoresistance (AMR) [8], planar Hall effect [9], tunnelling AMR (TAMR) [10–12] and Coulomb blockade AMR [13].

In spintronic applications, gallium manganese arsenide ((Ga,Mn)As) has been widely used as component for spin memory devices [9,14] using the magnetic anisotropy as one of the major physical quantities that determine the direction of the magnetization. The magnetic anisotropy in turn depends on many parameters, including temperature, carrier density and strain [1,15–18]. Epitaxially grown (Ga,Mn)As on GaAs has a compressive strain distribution in the (Ga,Mn)As region as a result of the lattice mismatch between the two materials. Spatial control of this strain field can be induced by lithographical etching. It generates a highly inhomogeneous strain-gradient distribution in the (Ga,Mn)As/GaAs structure. The inhomogenous strain gradient induces a static fourth-rank electric polarization field, which can be used to accumulate/deplete charge carriers in the device material upon application of an external electric field to such a system. The availability of the relevant method for precise studies of the spatial strain distribution in such systems is highly required. In this letter we report and focus on a coherent X-ray diffraction imaging technique to non-destructively retrieve the strain field in such device structures. Magnetic anisotropic quantities are predicted from the experimentally retrieved strain tensors.

X-ray data inversion analysis. – In case of crystalline objects the distribution of the X-ray scattered amplitude in reciprocal space around a reciprocal-lattice

(a) E-mail: andrey.minkevich@kit.edu

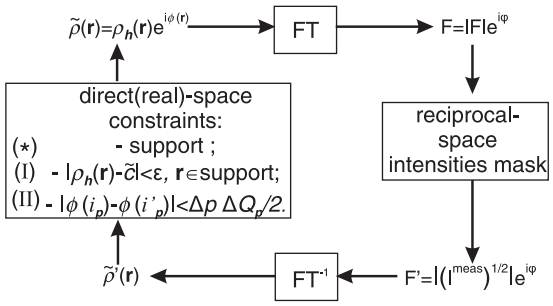

Fig. 1: Schematic diagram of the iterative loop of the proposed phase retrieval algorithm. $\tilde{c}$ corresponds to the arithmetic average of $\varrho_{\boldsymbol{h}}(\boldsymbol{r})$ within the support and ϵ defines the threshold of the electron density uniformity. i_p and i'_p are the neighbouring points along the p-direction (normally lateral or vertical) and Δp corresponds to the step along this direction (direct space resolution).

Point (RLP) is given by

$$E(\boldsymbol{Q}) \sim \int \mathrm{d}^3\boldsymbol{r} \left[\varrho_{\boldsymbol{h}}(\boldsymbol{r})\mathrm{e}^{-\mathrm{i}\boldsymbol{h}\boldsymbol{u}(\boldsymbol{r})}\right] \mathrm{e}^{-\mathrm{i}(\boldsymbol{Q}-\boldsymbol{h})\boldsymbol{r}}. \qquad (1)$$

This formula assumes the validity of the first Born approximation, thus the crystalline object has to be small. $\boldsymbol{h}$ and $\boldsymbol{Q}$ are the reciprocal-lattice vector and the position vector in reciprocal space (scattering vector), respectively, $\varrho_{\boldsymbol{h}}(\boldsymbol{r})$ is the corresponding Fourier component of non-strained periodic electron density and $\boldsymbol{u}(\boldsymbol{r})$ is the displacement field with respect to the non-strained lattice of bulk material. Once the phase of the scattered wavefield is known, the scatterer density distribution $\tilde{\varrho}(\boldsymbol{r}) = \varrho_{\boldsymbol{h}}(\boldsymbol{r})\exp(-\mathrm{i}\boldsymbol{h}\boldsymbol{u}(\boldsymbol{r}))$ (*i.e.* direct space amplitude $\varrho_{\boldsymbol{h}}(\boldsymbol{r})$ and phase $\boldsymbol{h}\boldsymbol{u}(\boldsymbol{r})$) can be obtained by inverse Fourier Transformation (FT). Since the phases are experimentally not accessible, the *direct* investigation of the shape and strain of the crystalline semiconductor device requires implementation of a phase retrieval method. The methodical principle is based on an iterative loop of direct and inverse FT (towards the experimental intensity distribution and back to the sample space) and it may refine the genuine scatterer density distribution $\tilde{\varrho}(\boldsymbol{r})$ even by starting with a non-realistic model [19,20].

An important step in the phase-retrieval method is the application of the constraints in reciprocal and direct (real) spaces (see [21,22], among others). In reciprocal space the constraints involve the routine replacement of the calculated amplitudes by the experimental ones at each iteration (see fig. 1). The direct-space constraint has a conventional form of an *a priori* specified support function determining the region in direct space, where the scatterer (electron) density may differ from zero. The method is on its way to become an established technique for reconstruction of the electron density of amorphous objects and unstrained crystals [23–27], since the problem is reduced to finding the amplitude information only (*e.g.*, $\tilde{\varrho}(\boldsymbol{r}) = \varrho_{\boldsymbol{h}}(\boldsymbol{r})$). In the case of a strained crystal, however, the situation is much more difficult. In diffraction calculations a model of the crystal is expressed by a set of complex values (see eq. (1)). Therefore there is a high probability for the inversion method to converge to false results [28]. Although the conventional phase retrieval method is applicable in the case of weakly inhomogeneous deformation fields [29], the problem persists in the case of high inhomogeneities [30]. Here we present the way to solve the outlined problem in the case of highly strained crystals by imposing complementary constraints in the iterative loop. The constraints are sequential from experimental data itself.

In the case of the unstrained crystal ($\boldsymbol{u}(\boldsymbol{r}) = 0$), it follows from eq. (1) that its diffraction pattern around the RLP is a FT of the crystal shape function. It corresponds to the narrow peak in reciprocal space with an intensity decay proportional to $|\boldsymbol{Q}-\boldsymbol{h}|^{-2}$ or higher. The full width of half maxima of the peak is proportional to the inverse of the crystal size. In contrast the presence of local strain gives rise to the strain-induced broad coherent diffuse scattering around the RLP. The width of signal broadening ΔQ around RLP (ΔQ_p —along arbitrary p-direction) is linearly proportional to the maximum displacement component gradient $\max\left[\frac{\partial \boldsymbol{h}\boldsymbol{u}(\boldsymbol{r})}{\partial r_p}\right]$ along the corresponding direction p. This fact allows to transform the "limited frequency constraint" into the direct space constraint of limited component of the displacement gradient. In addition it was found [30] that the constraint supporting the uniformity of the electron density in the frameworks of single crystal has to be introduced.

Therefore, we add two complementary direct-space constraints in addition to the standard support constraint (labeled by (I) and (II) in fig. 1). The constraint (I) requires that the amplitude $\varrho_{\boldsymbol{h}}(\boldsymbol{r})$ is uniform within the support area corresponding to the constituent crystal part. $\varrho_{\boldsymbol{h}}(\boldsymbol{r})$ tends to $\tilde{c}$, which is the average amplitude value in the support. The constraint (II) requires a continuity of the displacements. This means, that the phases which do not satisfy the constraint (II) are reset to the relevant values taken from the neighboring points. The direction p is usually chosen to point to the maximum displacement gradient (see marked ΔQ_p for (Ga,Mn)As part in fig. 2(c)). The outlined additional constraints (I)-(II) are required at the first iterations of the algorithm to bring the iterative process to the convergence. The final refinement is performed using only the support constraint, like it is done in conventional lensless microscopy.

The constraint (II) to the phases $\phi(\boldsymbol{r})$ (see fig. 1) assumes that the origin of our reciprocal-space Image (RSI) corresponds to the center of the strain-induced diffuse scattering cloud. The phases $\phi(\boldsymbol{r})$ in direct space are related to the displacement field via

$$\phi(\boldsymbol{r}) = \boldsymbol{h}\boldsymbol{u}(\boldsymbol{r}) + \Delta\boldsymbol{h}^{Bragg}\boldsymbol{r}, \qquad (2)$$

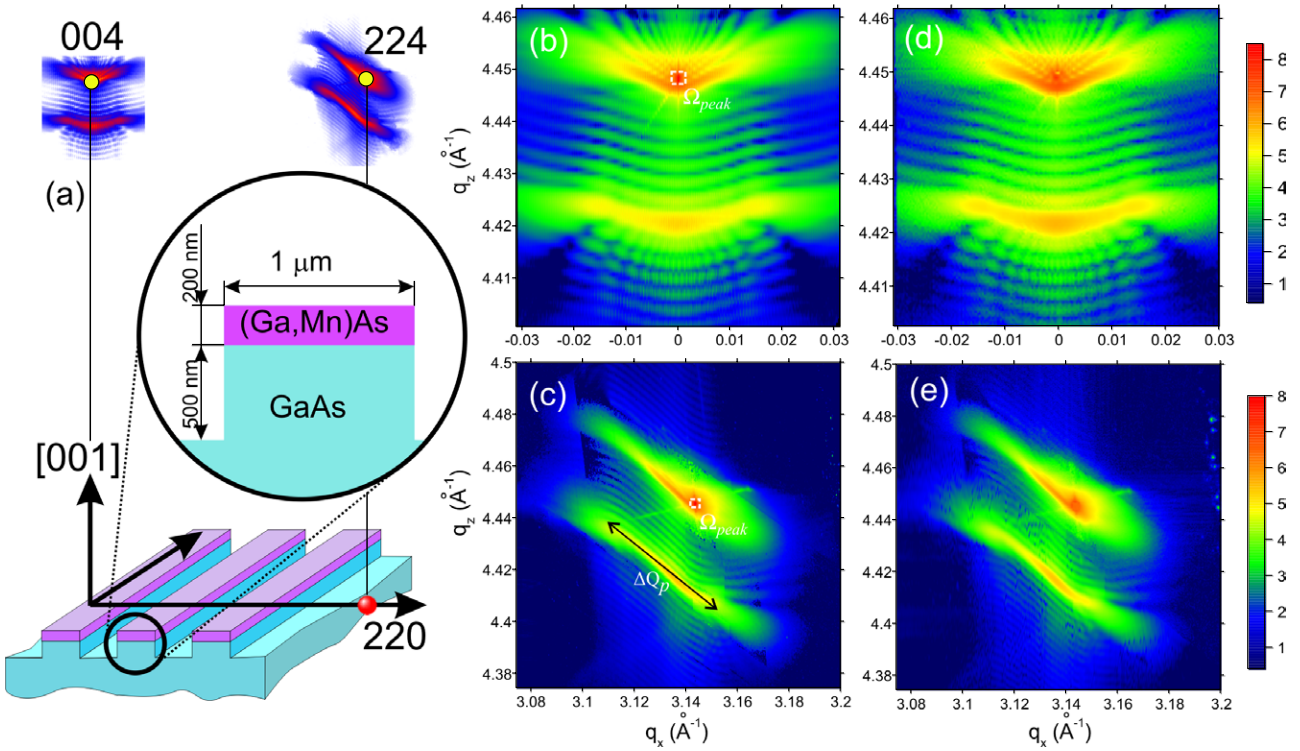

Fig. 2: (Colour on-line) (a) Schematic sketch of the (Ga,Mn)As/GaAs periodic wires and the RLPs measured during diffraction experiment. (b) Measured reciprocal-space map (logarithmic intensity scale) near 004 Bragg reflection from (Ga,Mn)As/GaAs periodic wires. (c) Measured data (like in (b)) near 224 Bragg reflection. (d) Calculated reciprocal-space map near 004 Bragg reflection from the results of reconstructions depicted in fig. 3(a). (e) Calculated data (like in (d)) near 224 Bragg reflection corresponding to the results in fig. 3(b).

where $\Delta \boldsymbol{h}^{Bragg}$ is a shift of origin of the RSI from the RLP corresponding to the ideal (non-deformed) reciprocal lattice described by $\boldsymbol{h}$.

Experimental. – We investigated a (Ga,Mn)As wire array with the period of $2\,\mu$m and the nominal wire width of $1\,\mu$m. A 200 nm thick (Ga,Mn)As layer with a nominal Mn concentration of about 7% was grown onto (001) GaAs substrate using molecular beam epitaxy. The periodic wire structure was prepared by electron beam lithography and reactive ion etching with an etching depth of approximately 700 nm (see fig. 2(a)). The (Ga,Mn)As surface wires are oriented along the $[1\bar{1}0]$ direction. The technological details can be found elsewhere [31].

The (Ga,Mn)As/GaAs wires represent a crystal structure with a two-dimensional distribution of the elastic displacement vector $\boldsymbol{u}(x,z)$ in the plane (x,z) perpendicular to the wire direction. The full inhomogeneous strain information in the wire can be reconstructed from two mutually independent Bragg reflections in the (x,z)-plane alone, since along the wire the strain in the layer is constant and corresponds to the lattice mismatch.

Diffraction measurements were performed at the ID10B and ID01 beamlines at ESRF, Grenoble, France. The X-rays from an undulator sources were monochromatized to $E = 8$ keV. Accurate retrieval of the strain field with high spatial resolution requires illumination by sufficiently high photon flux density. We used two experimental techniques to increase the strength of the scattering signal. In the first experiment at the ID10B beamline, the entire ensemble of identical wires was illuminated by a wide ($0.2 \times 0.2\,\mathrm{mm}^2$) partially coherent X-ray beam. High-resolution RSI in the vicinity of the 004 RLP (fig. 2(b)) was measured by use of a Si(111) crystal analyzer. The q_x-axis was perpendicular to the wires. The large coherence length exceeding the dimensions of one wire period allows for coherent magnifications of the scattering signal. In the second experiment at ID01 beamline, RSI around 224 RLP was measured (fig. 2(c)). The coherent photon flux was magnified at one single wire by a micro-focussing optic, consisting of a stack of beryllium compound refractive lenses. The data collection was performed using a Princeton CCD camera while rocking the sample around the axis parallel to the wires. Having some particularities, both techniques provide sufficiently good quality of experimental data for further direct treatment using a developed diffractive imaging method.

Results and discussion. – The diffraction peaks of the semi-infinite GaAs substrate in both of RSIs are described by the dynamical scattering theory. Since the reconstruction method is based on FT relation, assuming the validity of the kinematical approximation, it makes

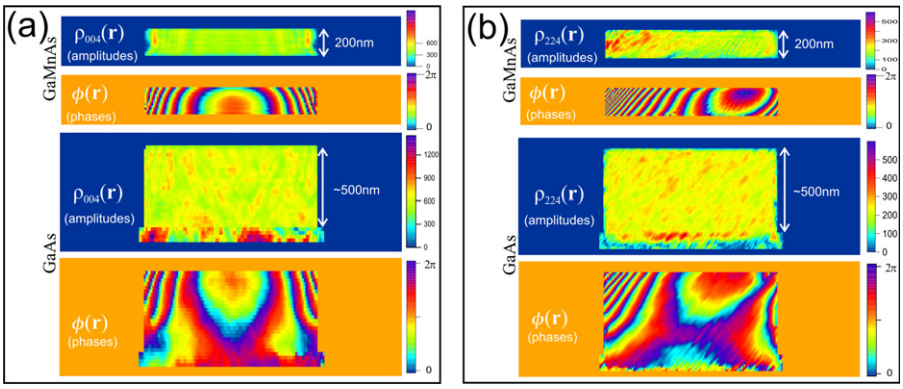

Fig. 3: (Colour on-line) (a) Results of the phasing method applied to the experimental data depicted in fig. 2(b). (e) Reconstruction of the diffraction pattern from fig. 2(c). The results for the (Ga,Mn)As and GaAs parts are shown separately.

sense to remove the substrate peak areas from the consideration. The eliminated experimental data near the GaAs RLP (marked by Ω_{peak} in both RSIs in fig. 2(b), (c)) is excluded from the reciprocal-space intensities mask constraint (see fig. 1) and allowed to vary freely during the reconstruction process. The RSIs data sampling corresponds to the horizontal dimensions of the direct space image being twice as large as the wire width. The signal oversampling in vertical direction is problematic because of the presence of the semi-infinite GaAs substrate and consequent absence of the bottom edge of the support in direct space. The diffuse scattering around the RLPs corresponds to the inhomogeneous deformation field in crystal. We reduced the vertical size of the support to fit to the deformed area, therefore, the oversampling requirements can be easily fulfilled.

The initial size of the support in direct space is chosen according to the technical specifications of the structure. Performing the phase-retrieval algorithm, the Fourier components of electron densities $\rho_{\boldsymbol{h}}(\boldsymbol{r})$ of (Ga,Mn)As and GaAs are assumed to be not affected by elastic deformation and shall vary only with composition.

The results of the phase retrieval reconstruction of the experimental data from fig. 2(b), (c) are depicted in fig. 3. The results for (Ga,Mn)As and GaAs are shown separately, since the corresponding RLPs are chosen to be different in each case. The RSIs in fig. 2(d), (e) calculated from the results of phase retrieval reconstruction (fig. 3) show good consistence with the experiment (fig. 2(b), (c)). The direct-space resolution achieved in $\Delta z \times \Delta x$ is about $10 \times 10\,\mathrm{nm}^2$ for the retrieved data from 004 RSI and twice as high —$5 \times 5\,\mathrm{nm}^2$— for 224 RSI.

The components of the displacement field are calculated from the reconstructed phases $\phi(\boldsymbol{r})$ shown in fig. 3 using eq. (2) starting from the unwrapped absolute phases. The 004 RSI provides us with the information about the relative vertical displacement component. The 224 RSI supplies us with the projections of the displacements on $\boldsymbol{h}^{224}$ and in combination with the vertical components it leads to the lateral components of displacements. The

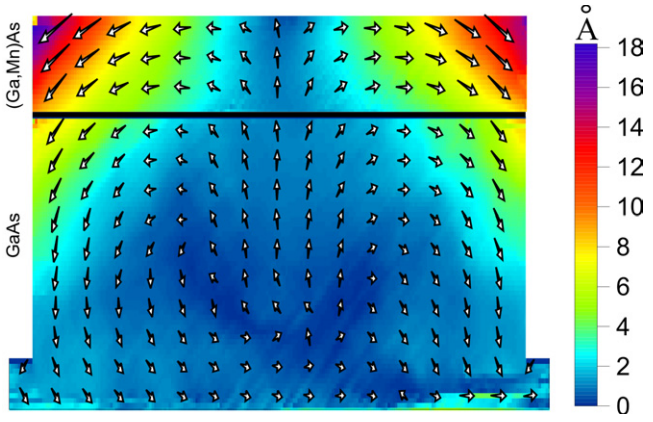

Fig. 4: (Colour on-line) Vector field of the atomic displacements (arrows not to scale) reconstructed directly from the X-ray data shown in fig. 2(b,c). The displacements are calculated from the phases shown in fig. 3. The magnitudes of the displacements are represented by the color map. For the structure dimensions see fig. 2(a).

vector field of the reconstructed atomic displacements is shown in fig. 4.

To further confirm the validity of our experimentally reconstructed strain tensor, we utilized the experimentally verified value (-0.35%) for the lattice mismatch between GaAs substrate and the (Ga,Mn)As layer containing 7% Mn as an input parameter for finite element analysis to model the strain tensor within our wire structure. The Poisson ratio and the Young modulus of GaAs were used as an approximation for (Ga,Mn)As. Boundary conditions for finite element simulations were specified by defining the stress on the borders of the Mn-containing layer. The top surfaces of GaAs substrate and the active layer where set free of stress. The results are in excellent agreement with the direct reconstruction results shown in fig. 4.

To maximize the functionality of spintronics devices based on (Ga,Mn)As, qualitative knowledge of the anisotropy components is required. These components

are usually described in energy terms using the phenomenological model which separates the free energy density into components having distinct symmetry [32]. Since the growth-induced strain is the strongest symmetry breaking mechanism, knowledge of this quantity is imperative. Therefore, we used the data of the reconstructed strain field to estimate the magnetic anisotropy in (Ga,Mn)As [33]. The value of the average lateral strain component, namely -0.14%, in (Ga,Mn)As (with the negative sign signifying compression) taken as input led the in-plane magnetocrystalline anisotropy coefficient to be in the range of 6.8–7.6 KJm^{-3} [34]. The result seems to be essentially larger than those received from experiments [10]. We think that the found discrepancies are caused by several factors. The first one is the possible restricted applicability of the phenomenological analysis [33] for the case of highly inhomogeneous deformations or given growth conditions [35]. Secondly, the influence of the manganese dopant concentration and subsequent solid solution micro- and meso-inhomogeneities may produce partial carrier localization effectively decreasing the experimentally observed anisotropy [2].

Conclusion. – In summary, we have demonstrated the capability of the coherent diffraction imaging phasing algorithm for the retrieval of the full strain tensor of relatively high magnitudes at nanoscale. We further show that such strain tensor information provides a gateway for a combined experimental-analytical non-destructive investigation of macroscopic energy density materials such as (Ga,Mn)As that can store, convert, and release energy (electrical, magnetic, and mechanical) in a well-controlled manner. The quantitative values of the displacement field reconstruction have been validated using the elasticity theory. The availability of a robust direct reconstruction method will allow to gain precise knowledge about multi-compositional strained nano-objects. Using the high quality of the reconstructed strain distribution, various applied properties, such as, magnetic anisotropy in (Ga,Mn)As can be directly estimated.

* * *

The work was supported by the NAMASTE project funded by the European Union. The authors thank A. Singh, O. Konovalov and A. Diaz for preparing the experimental setup. AAM and EF are very grateful to Prof. I. Robinson for the useful discussion and to J. Zemen of the group of Prof. T. Jungwirth.

REFERENCES

[1] Scherbakov A. V., Salasyuk A. S., Akimov A. V., Liu X., Bombeck M., Brüggemann C., Yakovlev D. R., Sapega V. F., Furdyna J. K. and Bayer M., *Phys. Rev. Lett.*, **105** (2010) 117204.

[2] Sawicki M., Chiba D., Korbecka A., Nishitani Y., Majewski J. A., Matsukura F., Dietl T. and Ohno H., *Nat. Phys.*, **6** (2010) 22.

[3] Dunsiger S. R., Carlo J. P., Goko T., Nieuwenhuys G., Prokscha T., Suter A., Morenzoni E., Chiba D., Nishitani Y., Tanikawa T., Matsukura F., Ohno H., Ohe J., Maekawa S. and Uemura Y. J., *Nat. Mater.*, **9** (2010) 299.

[4] Pappert K., Hümpfner S., Gould C., Wenisch J., Brunner K., Schmidt G. and Molenkamp L. W., *Nat. Phys.*, **3** (2007) 573.

[5] Zubko P., Catalan G., Buckley A., Welche P. R. L. and Scott J. F., *Phys. Rev. Lett.*, **99** (2007) 167601.

[6] Hong J., Catalan G., Scott J. F. and Artacho E., *J. Phys.: Condens. Matter*, **22** (2010) 112201.

[7] Matos-Abiague A. and Fabian J., *Phys. Rev. B*, **79** (2009) 155303.

[8] Wang K. Y., Edmonds K. W., Campion R. P., Zhao L. X., Foxon C. T. and Gallagher B. L., *Phys. Rev. B*, **72** (2005) 085201.

[9] Tang H. X., Kawakami R. K., Awschalom D. D. and Roukes M. L., *Phys. Rev. Lett.*, **90** (2003) 107201.

[10] Gould C., Rüster C., Jungwirth T., Girgis E., Schott G. M., Giraud R., Brunner K., Schmidt G. and Molenkamp L. W., *Phys. Rev. Lett.*, **93** (2004) 117203.

[11] Rüster C., Gould C., Jungwirth T., Sinova J., Schott G. M., Giraud R., Brunner K., Schmidt G. and Molenkamp L. W., *Phys. Rev. Lett.*, **94** (2005) 027203.

[12] Pappert K., Schmidt M. J., Hümpfner S., Rüster C., Schott G. M., Brunner K., Gould C., Schmidt G. and Molenkamp L. W., *Phys. Rev. Lett.*, **97** (2006) 186402.

[13] Wunderlich J., Jungwirth T., Kaestner B., Irvine A. C., Shick A. B., Stone N., Wang K.-Y., Rana U., Giddings A. D., Foxon C. T., Campion R. P., Williams D. A. and Gallagher B. L., *Phys. Rev. Lett.*, **97** (2006) 077201.

[14] Hamaya K., Taniyama T., Kitamoto Y., Moriya R. and Munekata H., *J. Appl. Phys.*, **94** (2003) 7657.

[15] Sawicki M., Matsukura F., Idziaszek A., Dietl T., Schott G., Ruester C., Gould C., Karczewski G., Schmidt G. and Molenkamp L., *Phys. Rev. B*, **70** (2004) 245325.

[16] Abolfath M., Jungwirth T., Brum J. and MacDonald A., *Phys. Rev. B*, **63** (2001) 54418.

[17] Dietl T., Ohno H. and Matsukura F., *Phys. Rev. B*, **63** (2001) 195205.

[18] Wenisch J., Gould C., Ebel L., Storz J., Pappert K., Schmidt M. J., Kumpf C., Schmidt G., Brunner K. and Molenkamp L. W., *Phys. Rev. Lett.*, **99** (2007) 077201.

[19] Fienup J. R., *Appl. Opt.*, **21** (1982) 2758.

[20] Elser V., *J. Opt. Soc. Am. A*, **20** (2003) 40.

[21] Vartanyants I. A. and Robinson I. K., *J. Phys.: Condens. Matter*, **13** (2001) 10593.

[22] Robinson I. and Harder R., *Nat. Mater.*, **8** (2009) 291.

[23] Miao J., Chen C.-C., Song C., Nishino Y., Kohmura Y., Ishikawa T., Ramunno-Johnson D., Lee T.-K. and Risbud S. H., *Phys. Rev. Lett.*, **97** (2006) 215503.

[24] Jiang H., Song C., Chen C.-C., Xu R., Raines K. S., Fahimian B. P., Lu C.-H., Lee T.-K., Nakashima A., Urano J., Ishikawa T., Tamanoi F. and Miao J., *Proc. Natl. Acad. Sci. U.S.A.*, **107** (2010) 11234.

[25] Schroer C. G., Boye P., Feldkamp J. M., Patommel J., Schropp A., Schwab A., Stephan S., Burghammer M., Schöder S. and Riekel C., *Phys. Rev. Lett.*, **101** (2008) 090801.
[26] Nishino Y., Takahashi Y., Imamoto N., Ishikawa T. and Maeshima K., *Phys. Rev. Lett.*, **102** (2009) 018101.
[27] Takahashi Y., Zettsu N., Nishino Y., Tsutsumi R., Matsubara E., Ishikawa T. and Yamauchi K., *Nano Lett.*, **10** (2010) 1922.
[28] Minkevich A. A., Gailhanou M., Micha J.-S., Charlet B., Chamard V. and Thomas O., *Phys. Rev. B*, **76** (2007) 104106.
[29] Pfeifer M. A., Williams G. J., Vartanyants I. A., Harder R. and Robinson I. K., *Nature*, **442** (2006) 63.
[30] Minkevich A. A., Baumbach T., Gailhanou M. and Thomas O., *Phys. Rev. B*, **78** (2008) 174110.
[31] Wunderlich J., Irvine A. C., Zemen J., Holý V., Rushforth A. W., De Ranieri E., Rana U., Výborný K., Sinova J., Foxon C. T., Campion R. P., Williams D. A., Gallagher B. L. and Jungwirth T., *Phys. Rev. B*, **76** (2007) 054424.
[32] Burenkov Y., Burdokov Y., Davidov S. and Nikanorov S., *Sov. Phys. Solid State*, **15** (1973) 1175.
[33] Zemen J., Kučera J., Olejník K. and Jungwirth T., *Phys. Rev. B*, **80** (2009) 155203.
[34] King C. S., Zemen J., Olejník K., Horák L., Haigh J. A., Novák V., Irvine A., Kučera J., Holý V., Campion R. P., Gallagher B. L. and Jungwirth T., *Phys. Rev. B*, **83** (2011) 115312.
[35] Gould C., Mark S., Pappert K., Dengel R. G., Wenisch J., Campion R. P., Rushforth A. W., Chiba D., Li Z., Liu X., Roy W. V., Ohno H., Furdyna J. K., Gallagher B., Brunner K., Schmidt G. and Molenkamp L. W., *New J. Phys.*, **10** (2008) 055007.